Nuclear spin noise imaging

Norbert Müller[†] and Alexej Jerschow[‡§]

[†]Institute of Organic Chemistry, Johannes Kepler University, Altenbergerstrasse 69, A-4040 Linz, Austria; and [‡]Department of Chemistry, New York University, 100 Washington Square East, New York, NY 10003

NMR images were obtained from the proton spin noise signals of a water-containing phantom, which was placed in the highly tuned, low-noise resonant circuit of a cryogenically cooled NMR probe in the presence of systematically varied magnetic field gradients. The spatially resolved proton spin density was obtained from the raw signal by a modified projection–reconstruction protocol. Although spin noise imaging is inherently less sensitive than conventional magnetic resonance imaging, it affords an entirely noninvasive visualization of the interior of opaque objects or subjects. Thus, tomography becomes possible even when neither x-ray nor radio frequency radiation can be applied for technical or safety reasons.

magnetic resonance imaging | radiation-free imaging | sensitivity

MRI is a powerful noninvasive tomographic technique. In medicine MRI is used as a versatile diagnostic tool offering superior contrast of soft tissue in the interior of the human body (1, 2). In addition, MRI is an important methodology in biological and material sciences (3). In conventional MRI, the subjects are placed in a uniform static magnetic field B_0 and irradiated with a series of high-power radio frequency (rf) pulses to excite coherent superpositions of spin states. Rapidly switched, spatially dependent magnetic fields (1, 2) are used to encode the spatial coordinates in the phases of the coherent states. These states induce a detectable signal in an rf coil arranged perpendicularly to the static magnetic field. The resonance frequencies can then be mapped to locations in space. One-dimensional profiles may be acquired quasicontinuously, and experiments with various magnetic field gradients along orthogonal axes are required to obtain two- and three-dimensional information. Either two- and three-dimensional Fourier transformation (3) or projection–reconstruction algorithms (4) are generally used to produce the images, in which the signal amplitude at particular frequency coordinates is proportional to the spin density at the corresponding location.

The major portion of the rf power applied in MRI and NMR spectroscopy (through, e.g., excitation pulses, refocusing pulses, and decoupling) is deposited within the sample as a result of resistive losses (5). Notwithstanding the potential direct effects of rf irradiation on living cells or tissue (6, 7), the primary biological effect is heating due to the thermogenic properties of the electromagnetic field. Therefore, safety regulations have been established for medical applications of MRI (8, 9) limiting the energy deposition in patients and medical staff. The working frequency ν_0 of MRI is linearly proportional to the applied magnetic field B_0, as given by the Larmor equation: $\nu_0 = \gamma B_0 / 2\pi$, where γ is the magnetogyric ratio of the observed nucleus (^{1}H for most applications). Although MRI at higher fields provides better sensitivity and better resolution, the rf power deposited in a dielectric sample increases approximately with the second power of the magnetic field and the second power of the rf field strength (5), causing technical problems and raising safety concerns.

Here, we report an MRI technique that does not require any form of external electromagnetic irradiation. The image acquisition is based on the detection of spontaneous spin noise in a tightly coupled, highly tuned rf circuit or cavity (10, 11). Apart from obviating the need to apply rf irradiation, spin noise signals do not require the existence of population differences between the nuclear spin states. Spin noise signals are relatively weak, but recent advances in rf detection systems make them measurable with commercially available equipment. Because the spin noise signals have a random phase, novel accumulation and processing protocols are required for image reconstruction.

Already shortly after the first experimental observation of the NMR phenomenon in condensed matter, Bloch (12) predicted that an ensemble of N spins, each carrying a magnetic moment μ, would induce tiny voltage fluctuations proportional to $N^{1/2}\mu$ in a surrounding coil, which could not be measured with the equipment available at that time. Sleator et al. (10, 11) achieved the first experimental observation of nuclear spin noise by detecting a weak nuclear quadrupole resonance noise spectrum of a sample cooled to 1.5 K in a tuned circuit using a superconducting quantum interference device (SQUID) detector. These researchers related the phenomenon of spin noise to spontaneous emission being enhanced by the coupling to cavity modes (10, 11). The low noise temperature offered by a SQUID detector combined with signal-averaging techniques made it possible to detect the spontaneous emission power, which is <10% of the Johnson–Nyquist noise power P_N generated in the same bandwidth as the spin noise, $P_N = 4k_B T \Delta\nu$, where k_B is the Boltzmann constant and $\Delta\nu$ is the bandwidth.

Later, Ernst and McCoy (13) and, independently, Guéron and Leroy (14) detected nuclear spin noise spectra from a sample at room temperature. Although their measurements were done with conventional rf probes of lower Q factors (300 and 115) than the SQUID ($Q \approx 4,000$) that had been used in the earlier experiments of Sleator et al. (10, 11), they achieved a higher signal-to-noise ratio in their room temperature experiments, mainly because of the low Johnson–Nyquist noise present in the narrow spectral width of $\Delta\nu = 0.2$ Hz. Ernst and McCoy (13) also assessed the role of radiation damping (15) in determining the features of spin noise. Guéron (16) subsequently described a simulation of a spin system by way of an equivalent electrical resonator and achieved a straightforward derivation of radiation damping and spin noise effects. More recently, Hoult et al. (17, 18) summarized the theory of spin noise and its historic development and described conditions for the detection of spin noise while minimizing radiation damping effects (17, 18). Nuclear spin noise has also been detected by using an optical Faraday rotation in alkali metal vapor (19). Electron spin noise was detected recently in the context of force-detected magnetic resonance (20, 21).

The rms value of the fluctuating magnetic moment, $N^{1/2}\mu$ (where $\mu = \gamma h I$) may be compared with the equilibrium moment for a spin ½ particle. In a magnetic field, B_0 under the high temperature approximation ($\hbar\gamma B_0/kT \gg 1$) the equilibrium ensemble moment is given by $N\mu(\mu B_0/kT)$ (14), which can be detected upon a $\pi/2$ pulse. The ratio between the two is
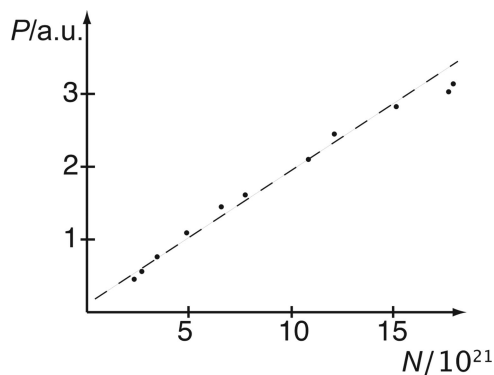
$$r = kT/(\mu B_0 N^{1/2}). \qquad [1]$$

Fig. 1. Dependence of the spin noise power signal P (arbitrary units) on the number of proton spins in the sample ($H_2O/{}^2H_2O$) measured with a room-temperature probe. The predicted linear relationship between noise power and the number of spins in the sample is observed. The different data points correspond to the various concentrations of H_2O in ${}^2H_2O$ that were tested.

For water in a typical active sample volume of 200 μl ($N = 1.34 \times 10^{22}$) at a field of $B_0 = 11.7$ T this factor amounts to $r = 3.4 \times 10^{-8}$. Because the signal-to-noise ratios of pulse-NMR experiments for such samples are in the range of 10^7 to 10^9, the spin noise signal should have a signal-to-noise ratio of close to unity and should therefore be measurable. The relationship of Eq. **1** also predicts more favorable ratios as the sample sizes become smaller. The ratio is, for example, on the order of unity for an ensemble of 1.6×10^7 spins.

Results and Discussion

The net power P transferred into a resonant circuit from a sample with N spins is (10, 11)

$$P \propto Q v N \gamma^2 / V_c. \qquad [2]$$

It is noteworthy that the population difference of the nuclear spin levels does not enter into this expression. Fig. 1 demonstrates the linear dependence of the spin noise power signal on the number of spins in a sample of constant volume.

For the reconstruction of spin noise images, we used a commercial liquid-state NMR spectrometer equipped with a cryogenically cooled probe (22, 23), where the rf coil and the preamplifier unit are cooled to 30 K and 77 K, respectively. The sample remains at 303.4 K. Although the application of magnetic field gradients is required to obtain spatial encoding, no rf pulses or irradiation are used.

Because the phase of the spin noise signals is random (10, 11), a coaddition of transients, which is required to enhance the signal-to-noise ratio, must follow a procedure different from the one used in the accumulation of conventional MRI or NMR signals. In the presence of a constant field gradient, the NMR noise can be digitized and recorded as a continuous sequence of packets. The duration of each packet corresponds to the acquisition time in conventional MRI and is determined by the desired resolution, whereas the digitization rate determines the spectral width, as usual. The individual packets are Fourier-transformed separately and coadded after calculation of the magnitude or power values of the complex data points. In this way, one obtains the power spectrum of the spin noise. As the noise signal amplitudes increase with the square root of the number of spins, the amplitudes in a power spectrum obey the same concentration proportionality as normal NMR signals (Fig. 1).

For two-dimensional imaging, a phantom as shown in Fig. 2a was used. Thirty one-dimensional images were acquired, with the direction of the transverse magnetic field gradient being rotated between successive experiments by 6° to cover a total
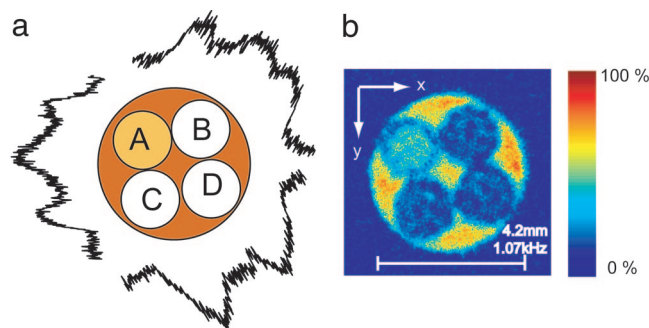
Fig. 2. Two-dimensional SNI of a phantom. (*a*) Phantom used for imaging (cross section). Three representative one-dimensional SNI are shown, which are arranged perpendicularly to the magnetic field gradient directions that were used to acquire them. (*b*) Two-dimensional SNI obtained from 30 one-dimensional images by projection–reconstruction.

of 180°. The peak-to-peak spin noise-to-thermal noise ratios were typically 20–25 for the individual one-dimensional images. After applying the projection reconstruction algorithm to this data set, the final two-dimensional image is obtained (Fig. 2b), which clearly depicts the geometry of the phantom and maps the distribution of ${}^1H$ nuclear spin densities in the phantom.

Much of the contrast in biomedical MRI is obtained from relaxation rate differences in addition to spin density differences. As can be expected, T_1 relaxation parameters do not have a bearing on the spin noise intensities (13). In contrast, T_2 (or T_2^*) contrast may be achieved through linewidth effects. We expect that additional image contrast can be obtained through nonlinear collective spin dynamics (24). More refined spin tagging or modulation of pixel intensities is possible through correlated measurements (25), which can be adapted for spin noise imaging (SNI).

Conclusions

The most salient feature of SNI is the absence of any form of external rf irradiation. Likewise, fast switching of strong magnetic field gradients is not required for the SNI approach. Therefore, mild imaging applications can be envisioned, and, in view of stricter safety regulations, those applications should be very appealing to the medical field. Further applications of this imaging approach may be found in the investigation of extremely delicate specimens, such as explosives. In addition, the independence of the signal strength from population differences between the spin levels may be advantageous for imaging systems in which longitudinal (T_1) relaxation times are extremely long or for situations in which imaging of saturated samples is required. In combination with other recent innovations of magnetic resonance technology, such as microTesla MRI (26, 27), unconventional light and mobile imaging apparatus could be constructed that do not expose the sample to either rf irradiation, strong magnetic fields, or fast-switched magnetic field gradients. The increased efficiency of spin noise detection for smaller spin ensembles (Eq. **1**) is of special interest in the context of NMR and electron paramagnetic resonance (EPR) microcoils like the ones used in microfluidic NMR (28). Furthermore, the spin noise detection principle could also be applied favorably to EPR imaging (29). Here, the square dependence on the gyromagnetic ratio in Eq. **2** together with the high-quality factors of EPR resonators would substantially increase the sensitivity, enabling totally new application areas for magnetic resonance microscopy.

APPLIED PHYSICAL SCIENCES

Materials and Methods

All NMR experiments were performed on a Bruker Avance spectrometer operating at 500 MHz. The power vs. spin noise relationship (Fig. 1) was verified on a room-temperature, triple-channel inverse probe ($Q = 125$ under tuned conditions) using a sample in which the H_2O fraction in ^2H_2O ratio was varied between 10% and 100%. Spin noise was acquired in 256 packets of 2,048 data points over a spectral window of 20 kHz. After Fourier transformation and power calculation, the individual packets were added. The number of spins in the samples was calibrated according to an estimate of the active volume of the receiver coil (18.8 mm, measured in a one-dimensional image) and an NMR tube inner diameter of 4.2 mm. The peak integral in a regular pulsed NMR experiment was used to obtain a measure for the relative number of spins in the sample.

The two-dimensional image featured in Fig. 2 was acquired by using the phantom as shown in Fig. 2*a*. Four glass capillaries (inner diameter, 1.2 mm; outer diameter, 1.56 mm) were inserted into a standard NMR tube (inner diameter, 4.2 mm; outer diameter, 5 mm), and the remaining space was filled with H_2O. One of the capillaries (capillary A) was filled with a 50% H_2O/^2H_2O mixture, and the other three were filled with 99.5% ^2H_2O. The experiments were performed with a cryogenic triple-resonance probe (^{1}H-^{13}C-^{15}N). Under tuned conditions for the H_2O protons, a quality factor $Q \approx 1,850$ was observed. To prevent any leakage or accidentally delivering rf power to the probe, the rf power transmission cable was disconnected. Thirty one-dimensional images were acquired, with the direction of the transverse magnetic field gradient being rotated in successive experiments by 6° to cover a total of 180°. The instrument's shim gradient coils were used for creating these gradients. The maximum achievable transverse gradient strength in this mode of operation was 0.6 G/cm (1 G = 0.1 mT). Each measured data packet was recorded with 2,048 acquisition points covering a spectral window of 5,000 Hz. A total of 512 packets were collected for each gradient setting and then coadded after Fourier transformation and magnitude calculation. The raw data acquisition took 52 min. Additional delays were used to allow sufficient time for the stabilization of the field gradients after each change of direction, increasing the total experiment time to ≈1 hr. The data set was then transformed with a filtered back-projection reconstruction algorithm based on the inverse Radon transform (4). Acquiring a "conventional image" (with pulsed excitation) of the same resolution (but much better signal to noise) takes ≈50 sec. The conventional imaging time increases with longer T_1 times. The repetition interval of the spin noise detected MRI experiment is, however, independent of relaxation times.

1. Lauterbur, P. C. (2004) in *The Nobel Prizes* 2003, ed. Frängsmyr, T. (Nobel Found., Stockholm), pp. 245–251.
2. Mansfield, P. (2004) in *The Nobel Prizes* 2003, ed. Frängsmyr, T. (Nobel Found., Stockholm), pp. 266–283.
3. Callaghan, P. T. (1991) *Principles of Nuclear Magnetic Resonance Microscopy* (Oxford Sci., Oxford).
4. Liang, Z.-P. & Lauterbur, P. C. (2000) *Principles of Magnetic Resonance Imaging: A Signal Processing Perspective* (IEEE, New York).
5. Bottomley, P. A. & Edelstein, W. A. (1981) *Med. Phys.* **8,** 510–512.
6. Kangarlu, A., Shellock, F. G. & Chakeres, D. (2003) *J. Magn. Reson. Imaging* **17,** 220–226.
7. Shellock, F. G. & Crues, J. V. (2004) *Radiology* **232,** 635–652.
8. U.S. Department of Health and Human Services, Food and Drug Administration, & Center for Devices and Radiological Health (2003) *Guidance for Industry and FDA Staff* (Food Drug Admin., Rockville, MD).
9. The European Parliament and the Council of the European Union (2004) *Off. J. Eur. Union* **L184,** 1–9.
10. Sleator, T., Hahn, E. L., Hilbert, C. & Clarke, J. (1985) *Phys. Rev. Lett.* **55,** 1742–1745.
11. Sleator, T. & Hahn, E. L. (1987) *Phys. Rev. B.* **36,** 1969–1980.
12. Bloch, F. (1946) *Phys. Rev.* **70,** 460–474.
13. McCoy, M. A. & Ernst, R. R. (1989) *Chem. Phys. Lett.* **159,** 587–593.
14. Guéron, M. & Leroy, J. L. (1989) *J. Magn. Reson.* **85,** 209–215.
15. Bloembergen, N. & Pound, R. V. (1954) *Phys. Rev.* **95,** 8–12.
16. Guéron, M. (1991) *Magn. Reson. Med.* **19,** 31–41.
17. Hoult, D. I. & Bhakar, B. (1997) *Concepts Magn. Reson.* **9,** 277–297.
18. Hoult, D. I. & Ginsberg, N. S. (2001) *J. Magn. Reson.* **148,** 182–199.
19. Crooker, S. A., Rickel, D. G., Balatsky, A. V. & Smith, D. L. (2004) *Nature* **431,** 49–52.
20. Boudakian, R., Mamin, H. J., Chui, B. W. & Rugar, D. (2005) *Science* **307,** 408–411.
21. Mamin, H. J., Budakian, R., Chui, B. W. & Rugar, D. (2003) *Phys. Rev. Lett.* **91,** 1–4.
22. Kovacs, H., Moskau, D. & Spraul, M. (2005) *Prog. Nucl. Magn. Reson. Spectrosc.* **46,** 131–155.
23. Styles, P., Soffe, N. F., Scott, C. A., Crag, D. A., Row, F., White, D. J. & White, P. C. J. (1984) *J. Magn. Reson.* **60,** 397–404.
24. Huang, S. Y., Akhtari, M., Mathern, G. W., Chute, D. J., Vinters, H. V., Datta, S., Walls, J. D. & Lin, Y.-Y. (2006) *Proc. Natl. Acad. Sci. USA,* in press.
25. Carson, P. J., Madsen, L. A., Leskowitz, G. M. & Weitekamp, D. P. (2000), U.S. Patents 6,078,872 and 6,081,119.
26. McDermott, R., Lee, S., Haken, B., Trabesinger, A. H., Pines, A. & Clarke, J. (2004) *Proc. Natl. Acad. Sci. USA* **101,** 7857–7861.
27. Myers, W. R., Mössle, M. & Clarke, J. (2005) *J. Magn. Reson.* **177,** 274–284.
28. Massin, C., Vincent, F., Homsy, A., Ehrmann, K., Boero, G., Besse, P.-A., Daridon, A., Verpoorte, E., de Rooij, N. F. & Popovica, R. S. (2003) *J. Magn. Reson.* **164,** 242–255.
29. Subramanian, S., Matsumoto, K.-I., Mitchell, J. B. & Krishna, M. C. (2004) *NMR Biomed.* **17,** 263–294.

Müller and Jerschow

www.manaraa.com